V International Scientific and Technical Conference Actual Issues of Power Supply Systems

Inhibition-Oriented Cognitively Informed Model-Free Adaptive Predictive PI Control for Delay- and Inertia-Dominated Nonlinear Processes: Robustness and Energy-Efficient Actuation

AIPCP25-CF-ICAIPSS2025-00335 | Article

Inhibition-Oriented, Cognitively Informed Model-Free Adaptive Predictive PI Control for Delay- and Inertia-Dominated Nonlinear Processes: Robustness and Energy-Efficient Actuation

Yusuf Avazov, Urinjon Choriev [a)], Elbek Ortikov, Jamshid Rakhimov

Tashkent state technical university named after Islam Karimov, Tashkent, Uzbekistan

[a)] *Corresponding author: chorievu95@mail.ru*

Abstract. Nonlinear industrial processes dominated by delay and inertia are difficult to regulate because sharp gain variations near sensitive regions, mixing/measurement dead time, and stochastic disturbances jointly produce overshoot, slow settling, and aggressive actuation. This paper presents an inhibition-oriented, cognitively informed model-free adaptive predictive PI controller that uses only online input–output data while explicitly promoting energy-aware actuation. The method (i) applies compact-form dynamic linearization to obtain a local incremental data model with an online pseudo-gradient estimate and multi-step prediction, (ii) incorporates a PI mechanism based on instantaneous tracking error and its accumulated sum – into the predictive optimization to suppress error build-up in delayed loops, and (iii) penalizes control increments to yield smoother inputs and lower actuator effort without compromising tracking speed. The controller is evaluated on a mechanistic nonlinear benchmark with a delay–inertia block (Figure 1–Figure 3) under set-point scheduling (Figure 5–Figure 6), delay-step changes (Figure 7), disturbance intensities (Figure 8; Table 3–Table 4), inertia variation (Figure 9; Table 5–Table 6), and tuning sensitivity (Figure 10–Figure 11). Relative to MFAC and conventional MFAPC baselines, it consistently reduces integrated and peak-error measures, achieving about 38–67% lower ISE, 20–48% lower IAE, and 40–50% lower maximum deviation across representative cases (Table 2–Table 6). The results suggest a robust, practically deployable route to high-performance regulation of delay- and inertia-dominated nonlinear processes with improved input economy.

INTRODUCTION

Nonlinear industrial plants dominated by transport/measurement delay and large inertia remain among the most difficult closed-loop regulation tasks. In chemical and environmental units, the input–output gain is highly nonuniform: wide regions respond weakly, while a narrow neighborhood becomes extremely sensitive, as reflected by a titration-type nonlinear characteristic (Figure 1) and the flow–mixing–reaction–measurement structure (Figure 2). When these nonlinearities combine with dead time and inertial dynamics (Figure 3), set-point changes and stochastic disturbances frequently produce overshoot, oscillations, and long settling times. Beyond tracking, plants increasingly require actuation economy because aggressive or oscillatory inputs increase energy use and accelerate wear, which is especially important in water and wastewater systems [1–2]. Although PID control is widespread, a single tuning rarely covers all operating regions in strongly nonlinear dead-time processes, making retuning or gain scheduling necessary [3–5]. Nonlinear MPC can systematically handle constraints and improve performance via prediction when an accurate, maintained model is available, yet modeling and continual updates are costly, and time-varying delay, unmodeled dynamics, and regime changes can erode robustness [6–7]. Intelligent methods (fuzzy, neuro-fuzzy, learning-based) reduce dependence on first-principles models and approximate nonlinear mappings [8], but stability/robustness under delay, inertia, and disturbances remains challenging [9]. Other nonlinear internal-model-based and evolutionary/GA-based designs can be effective in pH-type benchmarks, but often require strong assumptions or substantial tuning and add complexity, without always directly mitigating delay-driven error accumulation [10–13].

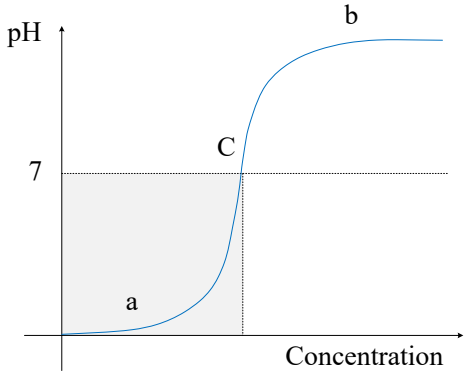

Figure 1. Nonlinear static characteristic with a high-gain jump near the nominal point.

Interest in data-driven, model-free adaptive control is increasing because it preserves adaptability without explicit mechanistic identification. Dynamic linearization provides a local incremental data model with an online pseudo-gradient inferred from input–output measurements [14–16]. Yet, when dead time dominates, delayed feedback can still produce overshoot and oscillatory inputs. Model-free adaptive predictive control introduces multi-step prediction and a tracking–effort compromise [17], but many schemes do not explicitly inhibit inter-sample error accumulation, which becomes decisive under large delay and inertia and can drive overly aggressive, energy-intensive actuation—particularly in variable pH regulation [18–19]. To address this gap, the paper proposes an inhibition-oriented, cognitively informed model-free adaptive predictive PI framework. It keeps dynamic linearization with online pseudo-gradient estimation, predicts the pseudo-gradient over the horizon via a recursive predictor [20], regulates both instantaneous and accumulated error through predictive PI action to suppress error build-up, and penalizes input increments to promote smooth, energy-aware actuation (Figure 4). Validation uses a mechanistic nonlinear benchmark with a delay–inertia block (Figure 1–Figure 3) and evaluates set-point tracking, delay/inertia sensitivity, disturbance robustness, and tuning effects (Figure 5–Figure 11; Table 2–Table 6).

EXPERIMENTAL RESEARCH

Experimental verification employs a reproducible nonlinear benchmark that captures industrial loops dominated by dead time and large inertia. It preserves a steep static gain variation, slow mixing/transport dynamics, and an explicit delay – features that commonly cause overshoot and oscillations under conventional regulation. The reactor interpretation follows Figure 2, the nonlinear sensitivity is shown in Figure 1, and the delay–inertia block matches Figure 3.

(a) Equivalent-state dynamics: To avoid numerical stiffness, the process is described by an equivalent surplus state $s(t)$(mol/L-equivalent), where $s(t) > 0$indicates acid dominance and $s(t) < 0$base dominance. For volume V, constant acid flow q_a, manipulated base flow $q_b(t)$, and inlet concentrations c_a, c_b, the well-mixed balance is

$$V\frac{ds(t)}{dt} = q_a(c_a - s(t)) - q_b(t)(c_b + s(t)). \quad (1)$$

(b) Nonlinear measurement transformation: The measured output is obtained through a nonlinear map derived from electroneutrality and water autoprotolysis. Denoting the water ion-product constant by K_w, the acidity index $y(t)$is computed from $s(t)$by

$$y(t) = \log_{10}\left(\frac{-s(t)+\sqrt{s^2(t)+4K_w}}{2K_w}\right). \quad (2)$$

This transformation generates the steep gain transition that motivates the inhibition objective, consistent with the sensitivity pattern in Figure 1.

(c) Discrete-time plant for controller evaluation: The benchmark is simulated under digital control with sampling period T_s. A forward discretization of (1) yields

$$s_{k+1} = s_k + \frac{T_s}{V}[q_a(c_a - s_k) - q_{b,k}(c_b + s_k)] + \varepsilon_k, \quad (3)$$

where $s_k = s(kT_s)$, $q_{b,k} = q_b(kT_s)$, and $\varepsilon_k$is an additive disturbance term capturing unmodeled effects and stochastic variability (its intensity is varied in later experiments). The discrete measured output follows

$$y_k = \log_{10}\left(\frac{-s_k+\sqrt{s_k^2+4K_w}}{2K_w}\right). \quad (4)$$

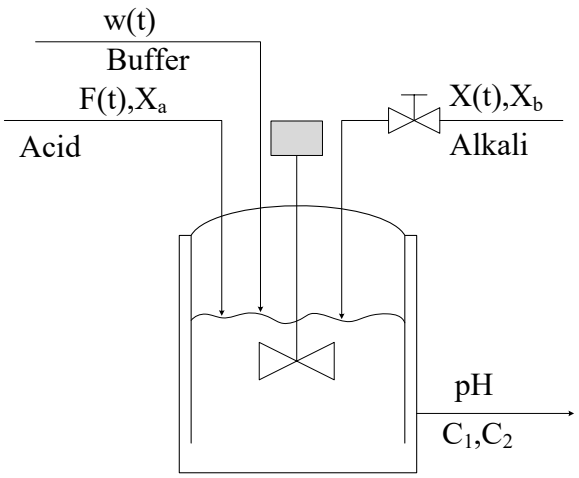

Figure 2. Stirred-tank mixing benchmark schematic with two inlets, buffering, and disturbance injection.

(d) Dead-time and inertia shaping of the manipulated channel: To reflect the fact that the control command affects the reactor only after transport, mixing, and measurement delays, an inertia–delay shaping block is introduced in the manipulated channel, consistent with Figure 3.

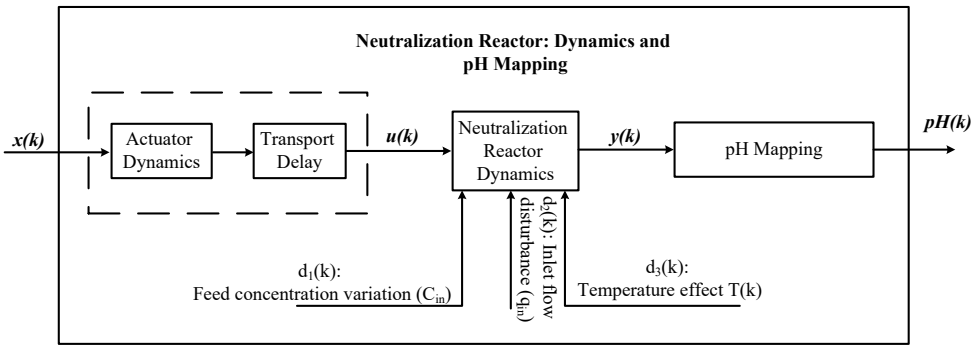

Figure 3. Delay–inertia nonlinear benchmark: input dynamics, process core, and static output mapping.

Let $u_k$be the controller command and $\bar{u}_k$the delayed/inertial plant input. With delay $d$and time constant τ,

$$\bar{u}_k = \rho\,\bar{u}_{k-1} + (1-\rho)\,u_{k-d}, \rho = \exp(-T_s/\tau). \quad (5)$$

In simulations, $q_{b,k} \leftarrow \bar{u}_k$. Experiments use nominal settings (Table 1) and a one-factor-at-a-time protocol: vary only one factor (set-point, delay, noise, inertia, or tuning) while keeping others fixed.

All experiments are executed in discrete time with sampling period T_s. The simulation plant is driven by the incremental state update

$$s_{k+1} = s_k + \frac{T_s}{V}[q_a(c_a - s_k) - q_{b,k}(c_b + s_k)] + \varepsilon_k, \quad (6)$$

and the measured output is computed via the nonlinear transformation

$$y_k = \log_{10}\left(\frac{-s_k+\sqrt{s_k^2+4K_w}}{2K_w}\right). \quad (7)$$

Table 1. Initial parameter settings of the benchmark model

Parameter	Symbol	Value	Unit
Inlet acid concentration	(c_a)	0.004	mol/L
Inlet alkali concentration	(c_b)	0.001	mol/L
Reactor (container) volume	(V)	20	L
Acid flow rate (constant)	(q_a)	0.25	L/min
Sampling time	(T_s)	1	min

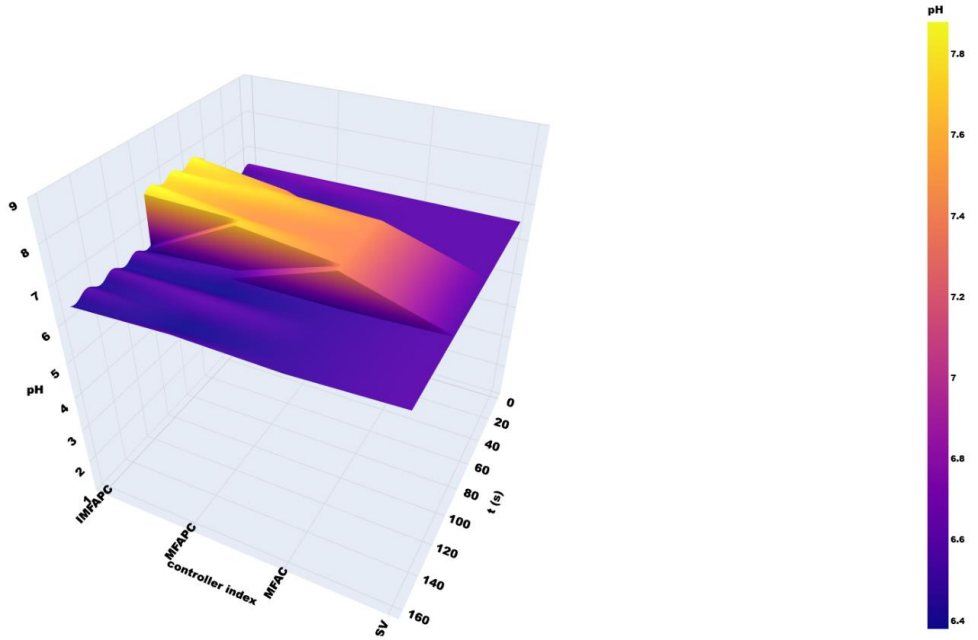

Figure 5. Moderate set-point tracking: MFAC, MFAPC, and inhibition-oriented predictive PI (reference band).

To represent transport/mixing and measurement effects, the manipulated input is filtered by an inertia–delay shaper. With controller command $u_k$and effective plant input $\bar{u}_k$, dead time $d$and time constant τ,

$$\bar{u}_k = \rho\,\bar{u}_{k-1} + (1-\rho)\,u_{k-d}, \rho = \exp\left(-\frac{T_s}{\tau}\right), \quad (8)$$

The plant in (6) is driven by $q_{b,k} \leftarrow \bar{u}_k$. States are initialized in a normal operating band to avoid artificial transients. A piecewise-constant reference $y_k^{\mathrm{ref}}$is applied using two schedules: intermediate-band (Figure 5) and wide-range across sensitivity regimes (Figure 6), with dwell times sufficient to expose transient and steady-state behavior.

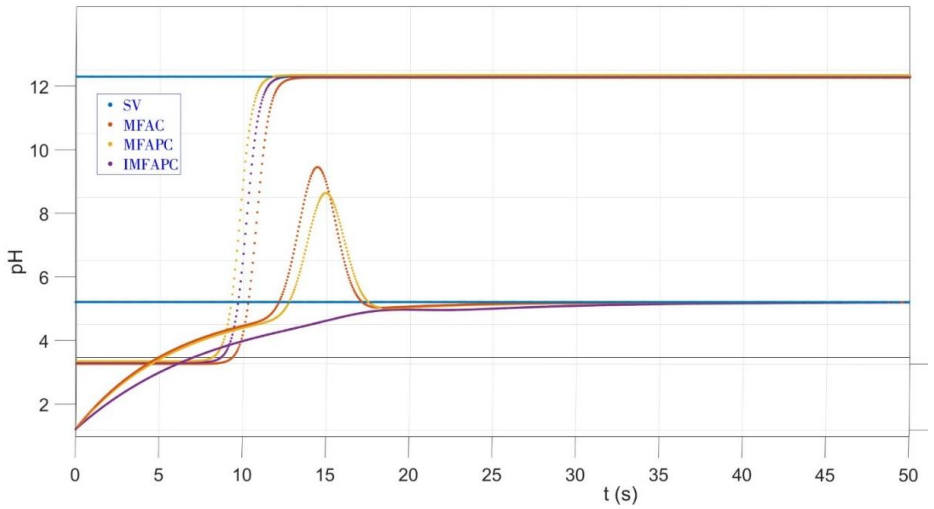

Figure 6. Wide-range pH step tracking (SV): MFAC, MFAPC, and IMFAPC.

The tracking error is defined as

$$e_k = y_k^{\mathrm{ref}} - y_k, \tag{9}$$

and the accumulated error used by the PI inhibition module is computed recursively as

$$\xi_k = \xi_{k-1} + T_s\, e_k, \xi_0 = 0. \tag{10}$$

Performance is quantified using three complementary indices that capture accuracy, robustness, and worst-case deviation over a finite horizon $k = 0, \ldots, K_f$:

$$\mathrm{ISE} = \sum_{k=0}^{K_f} e_k^2\ T_s, \mathrm{IAE} = \sum_{k=0}^{K_f} \mid e_k \mid\ T_s, \mathrm{MaxDev} = \max_{0 \le k \le K_f} \mid e_k \mid. \tag{11}$$

These criteria are used consistently across all scenarios and form the basis of the quantitative comparisons summarized later in Table 2–Table 6.

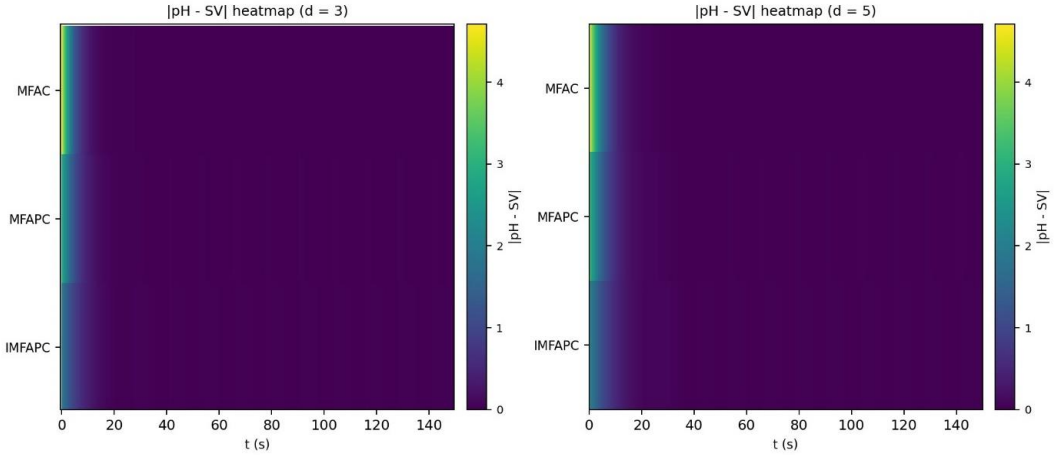

Figure 7. When the lag steps are 3 and 5, respectively.

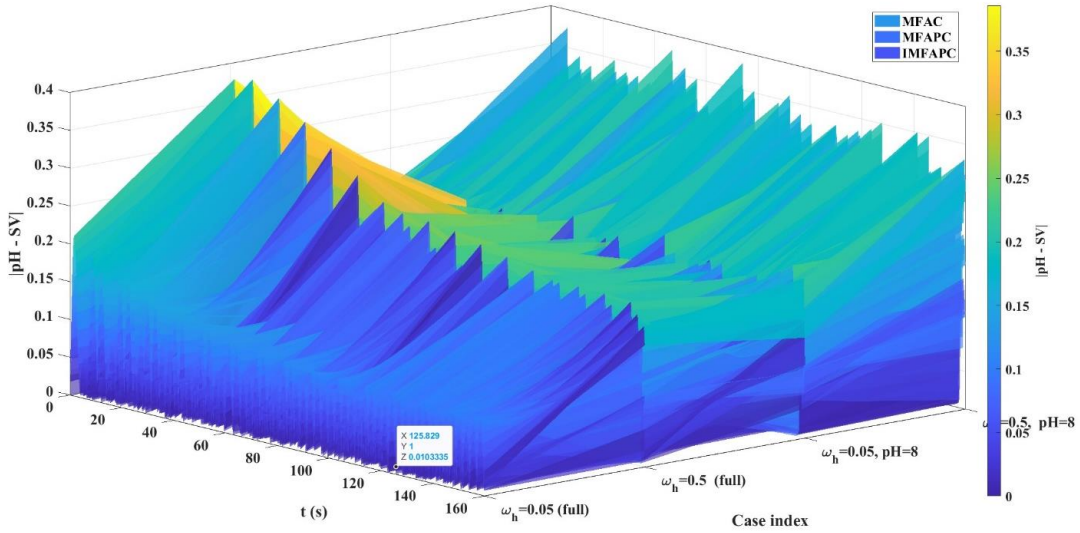

Figure 8. pH tracking for $T_P = 40$min, $d = 1$, $\phi(0) = 2$: effect of ω_k(0.05 vs 0.5) on MFAC/MFAPC/IMFAPC; lower panels zoom steady state.

Five experiment groups are conducted. (1) Baseline comparison under two set-point schedules benchmarks the proposed controller against two model-free baselines (Figure 5–Figure 6; Table 2). (2) Dead-time sensitivity varies the delay steps $d$in (5) (Figure 7). (3) Disturbance robustness adds zero-mean white noise $\varepsilon_k$in (3) at two intensities (Figure 8; Table 3–Table 4). (4) Inertia dominance varies τin (5) (Figure 9; Table 5–Table 6). (5) Tuning sensitivity sweeps predictive weights and pseudo-gradient initialization (Figure 10–Figure 11). All methods use the same discrete-time plant and the same inertia–delay input shaping (3)–(5), so differences reflect control laws only. Controllers compared: MFAC-type, MFAPC-type, and the proposed inhibition-oriented predictive PI.

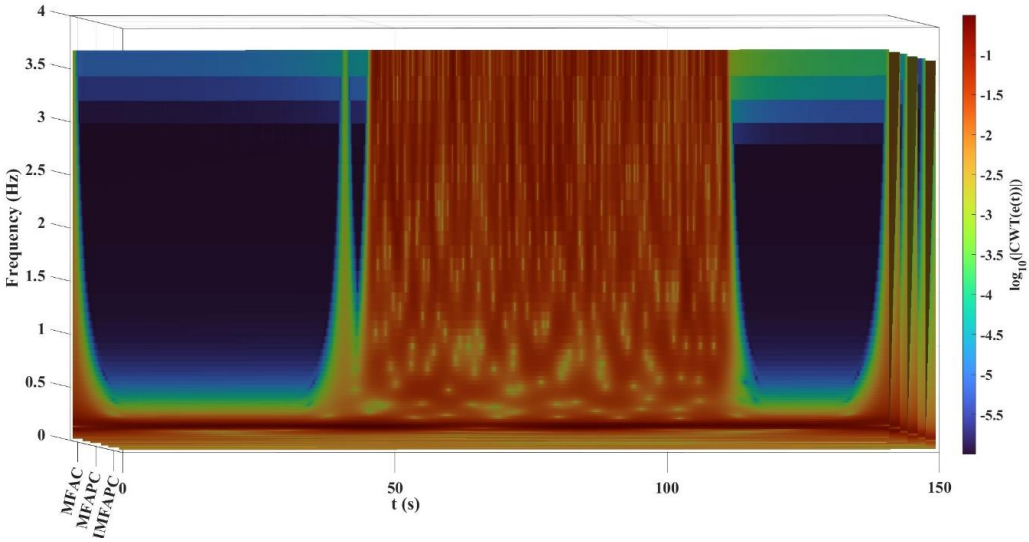

Figure 9a. Responses for $T_P = 50$and 100 min with $\phi(0) = 2$and $d = 1$.

The common modelling backbone for all data-driven methods is an incremental input–output representation built around the measured signal y_k. The increments are defined as

$$\Delta y_k = y_k - y_{k-1}, \Delta u_k = u_k - u_{k-1}. \quad (12)$$

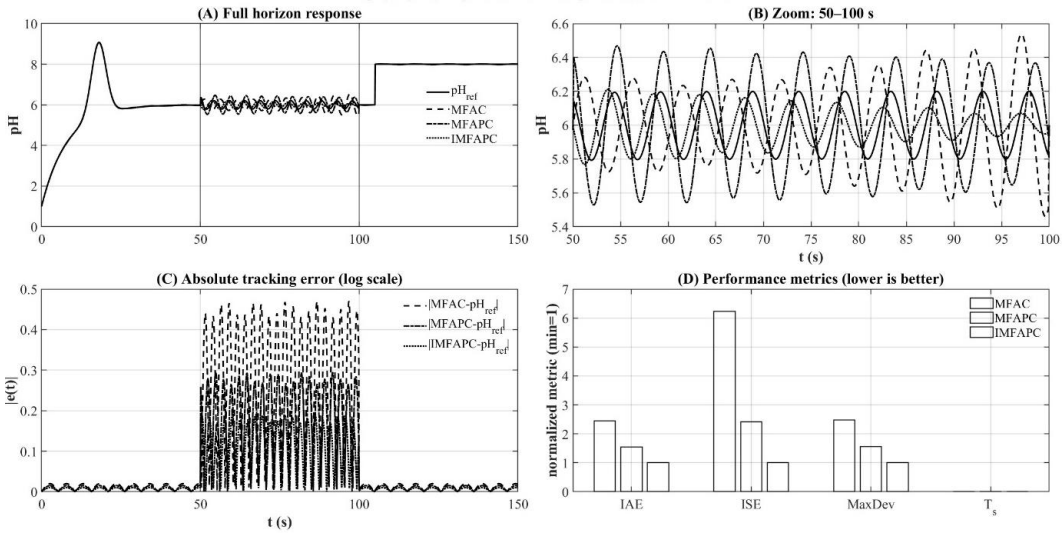

Figure 9b. System response when the inertia time of the system, TP is 50, 100 min, φ(0) = 2, d = 1.

Using compact-format dynamic linearization, the local incremental behavior along the operating trajectory is approximated by

$$\Delta y_{k+1} \approx \kappa_k \, \Delta u_k, \quad (13)$$

where $\kappa_k$is an unknown, time-varying pseudo-sensitivity that captures the local gain of the nonlinear plant. Since $\kappa_k$is not available a priori and varies with operating conditions, it is estimated online directly from input–output data via a normalized adaptation law:

$$\hat{\kappa}_k = \hat{\kappa}_{k-1} + \gamma \, \frac{\Delta u_{k-1}}{\sigma + \Delta u_{k-1}^2} (\Delta y_k - \hat{\kappa}_{k-1} \Delta u_{k-1}), \gamma \in (0,1]. \quad (14)$$

regularizes the update, preventing numerical degeneration when $\Delta u_{k-1}$is small and improving noise robustness. A safeguard resets the estimate to a positive initial value $\hat{\kappa}_{\text{init}}$whenever $| \Delta u_{k-1} |$ drops below a small threshold or $| \hat{\kappa}_k |$ becomes unrealistically small. For predictive schemes, future pseudo-sensitivities are obtained via a short autoregressive predictor fitted to recent $\hat{\kappa}$ estimates.

$$\hat{\kappa}_{k+j} = \sum_{i=1}^{p} a_{i,k} \; \hat{\kappa}_{k+j-i}, j = 1, \dots, N_c - 1, \quad (15)$$

where $p$is a small model order and $a_{i,k}$are time-varying predictor coefficients updated online via a regularized recursion. This yields horizon-dependent prediction matrices purely from data, without mechanistic modeling. Within this framework, the MFAC-type baseline updates the input using the instantaneous tracking error $e_k$in (9) and the current pseudo-sensitivity estimate, written in normalized form to prevent overly aggressive actuation when the estimated gain is small:

$$u_k = u_{k-1} + \beta_k \, \frac{\hat{\kappa}_k}{\lambda_0 + \hat{\kappa}_k^2} \, e_k, \quad (16)$$

where $\beta_k > 0$is a gain factor and $\lambda_0 > 0$is a regularization term that limits input excursions and improves stability in highly nonlinear regions. Over the control horizon, the future control increment vector is defined as $\Delta U_k = [\Delta u_k, \dots, \Delta u_{k+N_c-1}]^\top$, and the control sequence is determined by minimizing a quadratic criterion that trades off predicted tracking performance against input activity:

$$J_{\text{pred}} = \sum_{i=1}^{N_p} (\hat{y}_{k+i} - y_{k+i}^{\text{ref}})^2 + \lambda \sum_{j=0}^{N_c-1} \Delta u_{k+j}^2, \lambda > 0, \quad (17)$$

where $N_p$denotes the prediction horizon and $N_c$denotes the control horizon. The penalty λ is used to shape input smoothness and thus influence actuation economy.

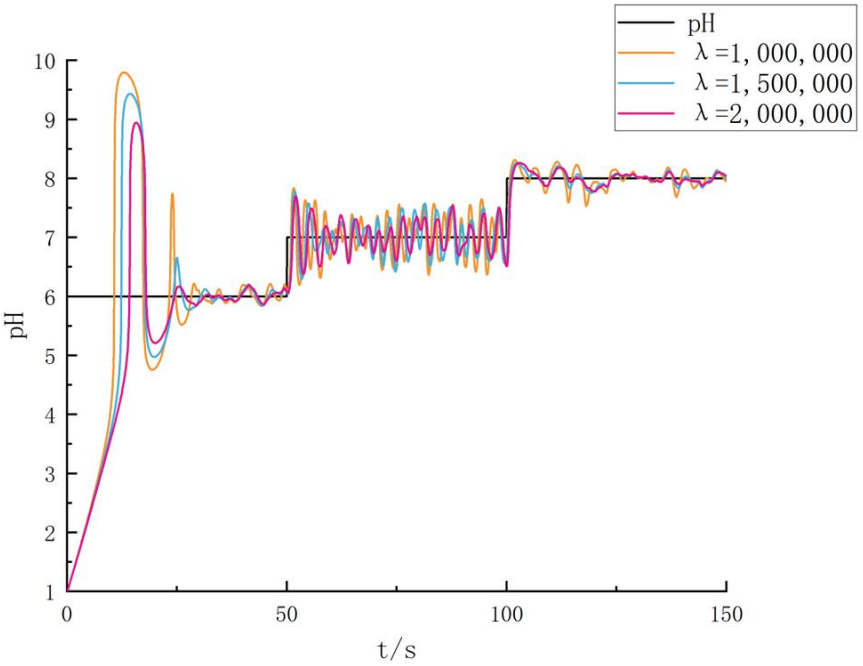

Figure 10. The control effect of IMFAPC under different λ.

The proposed inhibition-oriented predictive PI controller modifies the predictive objective by explicitly regulating the evolution of a PI-type error state, thereby suppressing error build-up that is exacerbated by dead time. Using the instantaneous error e_k(6) and the accumulated error ξ_k(7), the PI state is defined as

$$w_k = \begin{bmatrix} \xi_k \\ e_k \end{bmatrix}. \tag{18}$$

Under the incremental data model (10), the one-step evolution of this state can be expressed in a compact linear form:

$$w_{k+1} = A\, w_k + B_k\, \Delta u_k + C\, \Delta y_{k+1}^{\mathrm{ref}}, \tag{19}$$

Where,

$$A = \begin{bmatrix} 1 & T_s \\ 0 & 1 \end{bmatrix}, B_k = \begin{bmatrix} 0 \\ -\hat{\kappa}_k \end{bmatrix}, C = \begin{bmatrix} 0 \\ 1 \end{bmatrix}, \Delta y_{k+1}^{\mathrm{ref}} = y_{k+1}^{\mathrm{ref}} - y_k^{\mathrm{ref}}. \tag{20}$$

By propagating (16) over the control horizon and using the predicted pseudo-sensitivities from (12) to form the sequence $B_{k+1}, \dots, B_{k+N_c-1}$, a stacked prediction relationship is constructed:

$$W_k = \mathcal{G}\, w_k + \mathcal{F}_k\, \Delta U_k + \mathcal{H}\, \Delta Y_k^{\mathrm{ref}}, \tag{21}$$

with $W_k = [w_{k+1|k}^{\top}, \dots, w_{k+N_c|k}^{\top}]^{\top}$ and $\Delta Y_k^{\mathrm{ref}} = [\Delta y_{k+1}^{\mathrm{ref}}, \dots, \Delta y_{k+N_c}^{\mathrm{ref}}]^{\top}$. The control sequence is obtained by minimizing

$$J_{\mathrm{PIpred}} = \frac{1}{2} W_k^{\top} W_k + \frac{\lambda}{2} \Delta U_k^{\top} \Delta U_k, \tag{22}$$

which yields the closed-form optimizer

$$\Delta U_k^{\star} = -(\mathcal{F}_k^{\top} \mathcal{F}_k + \lambda I)^{-1} \mathcal{F}_k^{\top} (\mathcal{G}\, w_k + \mathcal{H}\, \Delta Y_k^{\mathrm{ref}}). \tag{23}$$

A receding-horizon strategy applies only the first move $\Delta u_k^{\star}$, updating

$$u_k = u_{k-1} + \Delta u_k^{\star}. \tag{24}$$

This makes inhibition explicit by shaping the predicted (ξ_k^m, e_k)dynamics, not only the output, while λlimits the size/variation of $\Delta u_k$to promote smooth, energy-aware actuation. Parameters (adaptation, regularization, horizons, λ) are fixed within each scenario (nominals in Table 1); tuning studies vary $\lambda$and $\hat{\kappa}_{\mathrm{init}}$(Figure 10–Figure 11), while other scenarios test delay steps (Figure 7), disturbances (Figure 8; Table 3–Table 4), and inertia changes (Figure 9; Table 5–Table 6).

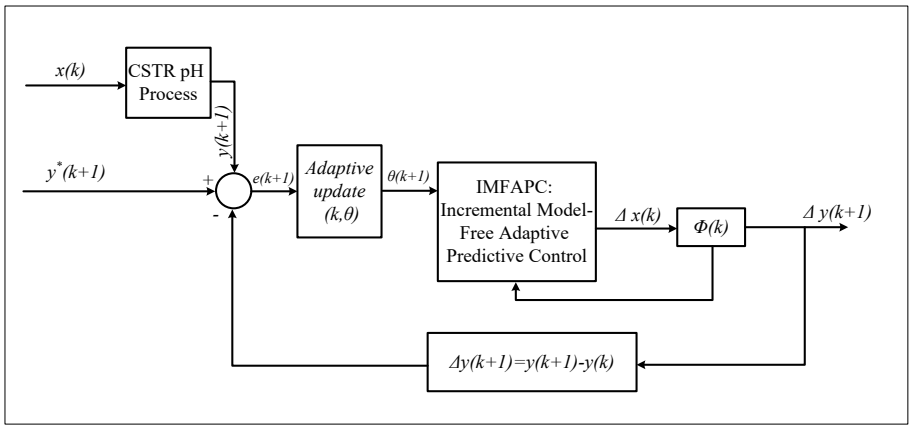

Figure 11. Closed-loop architecture of the inhibition-oriented model-free adaptive predictive PI controller.

All simulations use the same digital control loop. At each sample k, u_k is computed from current measurements/reference, shaped by the delay–inertia block (8) to $\bar{u}_k$, applied to the plant (3), and mapped to the measured output $y_k$via (7) over $k = 0, \dots, K_f$; indices are computed consistently. To ensure fairness and avoid numerical issues in sensitive regions, identical constraints are imposed for all controllers: input saturation:

$$u_k^{\text{sat}} = \min\left(u_{\max}, \max\left(u_{\min}, u_k\right)\right), \tag{25}$$

and increment (rate) saturation:

$$\Delta u_k^{\text{sat}} = \min\left(\Delta u_{\max}, \max\left(\Delta u_{\min}, \Delta u_k\right)\right), u_k^{\text{sat}} = u_{k-1}^{\text{sat}} + \Delta u_k^{\text{sat}}. \tag{26}$$

Disturbances enter via $\varepsilon_k$in (3); robustness tests use

$$\varepsilon_k \sim \mathcal{N}(0, \sigma_\varepsilon^2) \qquad \varepsilon_k \sim \mathcal{N}(0, \sigma_\varepsilon^2), \tag{27}$$

with σ_ε^2 set per Figure 8 and Table 3–Table 4. The same random seed is used across controllers within each scenario to apply identical disturbance realizations.

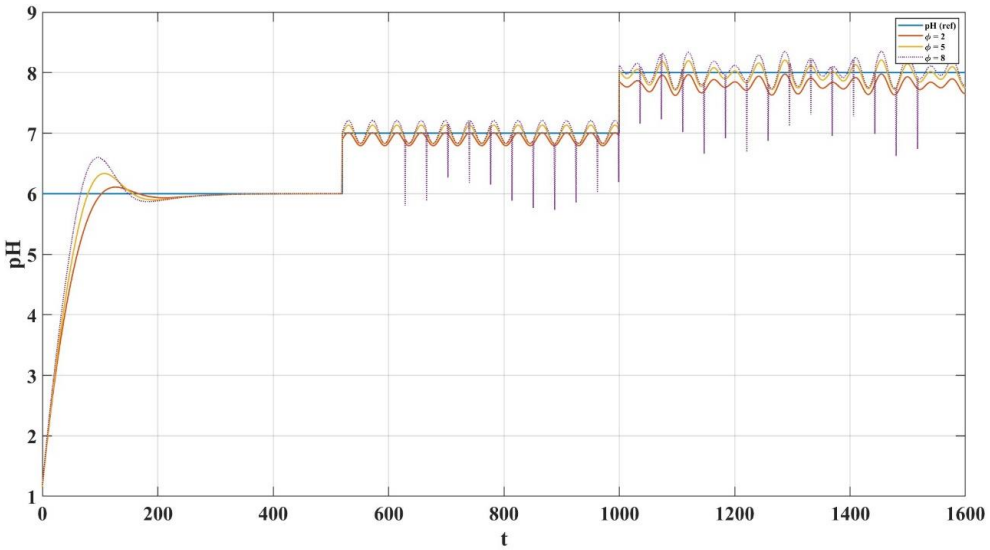

Figure 12. The rest of the conditions are the same as the simulations of IMFAPC with different φ.

Sensitivity analysis sweeps key parameters. The predictive weight λ in (14) and (19) is varied to reveal the aggressiveness–overshoot trade-off (Figure 10), while $\hat{\kappa}_{\text{init}}$ and the regularization terms in (11) are varied to assess

pseudo-sensitivity convergence and closed-loop robustness under different initial gain assumptions (Figure 11). For each setting, the same reference y_k^{ref} is applied, and e_k and ξ_k are computed consistently via (6)–(7) (and the PI-state recursion) across runs. Results are reported as time trajectories (Figure 5–Figure 9) to judge overshoot/settling/oscillations and as scalar indices (8) in Table 2–Table 6 to rank controllers by integrated deviation, error accumulation, and worst-case deviation, ensuring transparent and reproducible evaluation aligned with robustness and energy-aware actuation.

RESEARCH RESULTS

MFAC, MFAPC, and the proposed inhibition-oriented predictive PI controller are compared under scheduled set-point changes with nominal delay–inertia and baseline disturbance (Table 1) on the same plant (3)–(5) using (8). In Figure 5, the proposed method reaches set-points faster with much less overshoot; MFAC shows the largest delay-driven transients, and MFAPC improves but retains residual overshoot and oscillatory tails in the sensitive region. By regulating the predicted error state $w_k = [\xi_k, e_k]^{\mathrm{T}}$(15)–(17), it achieves the lowest ISE, IAE, and MaxDev (Table 2). In Figure 6, as the operating range widens, MFAC/MFAPC degrade under nonlinear gain variation, while the proposed controller maintains stable tracking with a tighter response envelope via online pseudo-sensitivity prediction and PI-state inhibition.

Table 2. Dynamic performance comparison (baseline step-tracking scenarios)

Controller	ISE	IAE	MaxDev
MFAC	0.160	0.301	1.954
MFAPC	0.114	0.246	1.698
Proposed (IMFAPC)	0.071	0.192	1.013

Figure 5–Figure 6 and Table 2 show that the inhibition-oriented predictive PI controller achieves the best set-point tracking on the nonlinear delay–inertia plant, improving accuracy and reducing overshoot versus MFAC and MFAPC. Robustness tests on the same setup (3)–(5), (8) indicate that increasing delay steps $d$degrades all responses (Figure 7), with MFAC worsening most due to delay-driven correction build-up and MFAPC retaining oscillatory tails without explicit error-inhibition. The proposed method stays tighter by forecasting and penalizing $w_k = [\xi_k, e_k]^{\mathrm{T}}$ (16)–(20), limiting ξ_k growth and suppressing over-corrections. With stronger white-noise ε_k in (3), fluctuations increase (Figure 8) but the proposed controller degrades least because PI-state prediction smooths actions; Table 3–Table 4 confirm the lowest ISE/IAE and smallest MaxDev. The third group then analyzes increased inertia and tuning trade-offs among speed, overshoot suppression, robustness, and input economy.

Table 3. Dynamic performance comparison at disturbance level $\omega_k = 0.05$

Controller	ISE	IAE	MaxDev
MFAC	0.096	0.196	1.904
MFAPC	0.068	0.159	1.608
Proposed (IMFAPC)	0.042	0.127	1.009

Table 4. Dynamic performance comparison at disturbance level $\omega_k = 0.5$

Controller	ISE	IAE	MaxDev
MFAC	0.260	0.340	2.022
MFAPC	0.203	0.350	1.848
Proposed (IMFAPC)	0.120	0.265	1.019

Inertia dominance is evaluated by increasing the time constant τin the input shaping (5) while keeping d and other parameters fixed. As shown in Figure 9, larger τ makes the loop more sluggish, increasing overshoot and recovery time when controllers compensate for slow response. MFAC exhibits the largest overshoot because error-driven corrections accumulate before the inertial element delivers the command to the plant. MFAPC reduces overshoot but retains residual deviation and slower damping. The proposed inhibition-oriented predictive PI controller achieves the lowest overshoot and a more monotone convergence, especially in the most sensitive operating region.

Table 5. Dynamic performance comparison at inertia time constant $T_P = 50$

Controller	ISE	IAE	MaxDev
MFAC	0.109	0.219	1.925
MFAPC	0.072	0.165	1.646
Proposed (IMFAPC)	0.044	0.131	1.009

Table 6. Dynamic performance comparison at inertia time constant $T_P = 100$

Controller	ISE	IAE	MaxDev
MFAC	0.174	0.293	2.035
MFAPC	0.102	0.207	1.778
Proposed (IMFAPC)	0.057	0.151	1.009

This behavior follows from PI-state prediction in (16)–(20): forecasting the coupled evolution of ξ_k and e_k discourages repeated moves under inertial lag and prevents "late overshoot" when stored control effort is released. Table 5–Table 6 support Figure 9: although error indices increase with τ for all controllers, the proposed method consistently achieves the lowest ISE, IAE, and MaxDev. Reducing MaxDev is especially critical at high inertia because peak excursions drive large corrective actions and higher actuator/energy loading; limiting peaks while keeping integrated error low yields a more stable, energy-aware envelope. Tuning results highlight the aggressiveness–smoothness trade-off. The predictive weight λ in (14) and (19) penalizes Δu_k: smaller λ accelerates transients but increases overshoot, whereas larger λ suppresses overshoot at the cost of slower response and possible residual error during fast set-point changes (Figure 10). The inhibition-based formulation offers a better compromise – similar overshoot with less input activity – because PI-state prediction limits error accumulation rather than relying on repeated large increments. Figure 11 shows that larger $\hat{\kappa}_{\text{init}}$ speeds the initial response but can reduce stability if the assumed gain is too high; an intermediate initialization is most reliable, after which (11) refines $\hat{\kappa}_k$. Once $\hat{\kappa}_k$ is reasonable, PI-state regulation (16)–(20) prevents estimation errors from producing excessive increments. Overall, Figure 9–Figure 11 and Table 5–Table 6 demonstrate robustness under increased inertia and interpretable tuning of the speed–overshoot–economy trade-off, with lower integrated error, smaller peaks, and smoother actuation.

CONCLUSIONS

This study proposed an inhibition-oriented, model-free adaptive predictive PI controller for nonlinear processes with pronounced dead time and strong inertia. A mechanistically interpretable, computationally tractable benchmark combined discrete-time nonlinear dynamics, a strongly nonlinear measurement map, and an explicit inertia–delay shaping block. The controller is built purely from input–output data using online pseudo-sensitivity estimation with short-horizon prediction, while its key novelty is regulating a predicted PI-type error state to inhibit error accumulation that typically drives overshoot and oscillations in delayed loops. Across set-point schedules, the proposed method produced tighter tracking and consistently lower overshoot than MFAC-type and MFAPC-type baselines, confirmed in Figure 5–Figure 6 and Table 2. Robustness tests showed the inhibition mechanism remains effective as delay steps increase and disturbance intensity rises, yielding smaller deviation envelopes and lower cumulative error under both noise levels (Figure 7–Figure 8, Table 3–Table 4). With increased inertia, it suppressed "late overshoot" and maintained stable convergence, achieving the best overall indices (Figure 9, Table 5–Table 6). Tuning studies

highlighted practical trade-offs: the predictive weight sets input aggressiveness, and pseudo-sensitivity initialization affects early transients, enabling selection of a balance among speed, overshoot inhibition, robustness, and actuation economy (Figure 10–Figure 11). By embedding accumulated-error dynamics in the predictive objective, the approach reduces repeated large corrective increments, supporting resource-aware, energy-efficient operation.

Limitations include reliance on offline parameter/horizon sweeps; an online auto-tuning mechanism would strengthen deployment. Future work will test additional process units with different nonlinearities and disturbance structures and address real-time implementation constraints, including computation limits and actuator bounds, to further establish industrial applicability.

REFERENCES

1. Li J, Tang Z, Luan H, Liu Z, Xu B, Wang Z, He W. An improved method of model-free adaptive predictive control: a case of pH neutralization in WWTP. *Processes*. 2023;11(5):1448. doi:10.3390/pr11051448.
2. Zhang S, Zhou P, Xie Y, Chai T. Improved model-free adaptive predictive control for direct data-driven control of a wastewater treatment process. *J Process Control*. 2022;110:11–23. doi:10.1016/j.jprocont.2021.11.015.
3. Hou Z, Jin S. A novel data-driven control approach for a class of discrete-time nonlinear systems. *IEEE Trans Control Syst Technol*. 2011;19(6):1549–1558. doi:10.1109/TCST.2010.2093136.
4. Hou Z, Chi R, Gao H. Dynamic-linearization-based data-driven control and applications: an overview. *IEEE Trans Ind Electron*. 2017;64(5):4076–4090. doi:10.1109/TIE.2016.2636126.
5. Mukhitdinov D, Kadirov Y, Sultanov I, Avazov Y. Rectification process control by separation process efficiency evaluation using a predictive model. *EPJ Web Conf*. 2025;321:01013. doi:10.1051/epjconf/202532101013.
6. Yusupbekov N, Avazov Y, Samadov E, Khojiyeva N, Shodiev M, Bazarbaev Q. Study of the technological process of vegetable oil refining as an object of monitoring, control and management. *AIP Conf Proc*. 2025;3268:040044. doi:10.1063/5.0257158.
7. Avazov Y, Shodiev M, Rajabov A, Turaev K. Control of the lifecycle of a technological complex for rectification of multicomponent mixtures under parameter uncertainty. *E3S Web Conf*. 2023;417:05010. doi:10.1051/e3sconf/202341705010.
8. Shodiyevich AY. Governance model the stochastic process of rectification of multicomponent mixtures based on fuzzy logic. In: Aliev RA, Yusupbekov NR, Kacprzyk J, Pedrycz W, Sadikoglu FM, eds. *Advances in Intelligent Systems and Computing*. Vol 1323. WCIS 2020. Springer; 2021. doi:10.1007/978-3-030-68004-6_48.
9. Gulyamov S, Avazov Y, Samadov E, Khojiyeva N, Bazarbaev Q. Some issues of increasing energy efficiency of advanced process and production control systems. *AIP Conf Proc*. 2025;3331(1):060009. doi:10.1063/5.0305712.
10. Kulkarni BD, Tambe SS, Shukla NV, Deshpande PB. Nonlinear pH control. *Chem Eng Sci*. 1991;46(4):995–1003. doi:10.1016/0009-2509(91)80083-J.
11. Mwembeshi MM, Kent CA, Salhi S. Genetic-algorithm-based intelligent modelling and control of pH in reactors. *Comput Chem Eng*. 2004;28(9):1743–1757. doi:10.1016/j.compchemeng.2004.04.009.
12. Tan WW, Lu F, Loh AP, Tan KC. Modeling and control of a pilot pH plant using genetic algorithm. *Eng Appl Artif Intell*. 2005;18(4):485–494. doi:10.1016/j.engappai.2004.11.006.
13. Wu H, Yan F, Wang G, Lv C. Decentralized fuzzy-inference-based predictive control for a pH neutralization process. *J Process Control*. 2022;110:76–83. doi:10.1016/j.jprocont.2021.12.001.
14. Sha'aban YA, Tahir F, Masding PW, Mack J, Lennox B. Control improvement using MPC: pH control for brine dechlorination. *IEEE Access*. 2018;6:13418–13428. doi:10.1109/ACCESS.2018.2810813.
15. Zeng J, Liu J. Economic model predictive control of wastewater treatment processes. *Ind Eng Chem Res*. 2015;54(22):5710–5721. doi:10.1021/ie504995n.
16. Zhang Y, Yin X, Liu J, Zeng J. Distributed economic model predictive control of wastewater treatment plants described by the Benchmark Simulation Model. *Chem Eng Res Des*. 2019;141:144–155. doi:10.1016/j.cherd.2018.10.039.
17. Shen W, Chen X, Corriou JP. Model predictive control of the Benchmark Simulation Model of a wastewater treatment process. *Comput Chem Eng*. 2008;32(12):2849–2856. doi:10.1016/j.compchemeng.2008.01.009.
18. Ma YS, Che WW, Deng C, Wu ZG. Dynamic event-triggered model-free adaptive control for nonlinear CPSs under aperiodic DoS attacks. *Inf Sci*. 2022;589:790–801. doi:10.1016/j.ins.2022.01.009.
19. Zhang B. Prescribed-performance model-free adaptive sliding-mode constrained control for a class of nonlinear systems. *Inf Sci*. 2021;544:97–116. doi:10.1016/j.ins.2020.06.061.